

LABORATORY STUDIES ON THE FORMATION OF FORMIC ACID (HCOOH) IN INTERSTELLAR AND COMETARY ICES

CHRIS J. BENNETT^{1,2}, TETSUYA HAMA^{3,5}, YONG SEOL KIM¹, MASAHIRO KAWASAKI³, AND RALF I. KAISER^{1,2,4}

¹ Department of Chemistry, University of Hawaii, Honolulu, HI 96822, USA; ralfk@hawaii.edu

² NASA Astrobiology Institute, University of Hawaii, Honolulu, HI 96822, USA

³ Department of Molecular Engineering, Kyoto University, Kyoto 615-8510, Japan

Received 2010 July 9; accepted 2010 October 5; published 2010 December 29

ABSTRACT

Mixtures of water (H₂O) and carbon monoxide (CO) ices were irradiated at 10 K with energetic electrons to simulate the energy transfer processes that occur in the track of galactic cosmic-ray particles penetrating interstellar ices. We identified formic acid (HCOOH) through new absorption bands in the infrared spectra at 1690 and 1224 cm⁻¹ (5.92 and 8.17 μm, respectively). During the subsequent warm-up of the irradiated samples, formic acid is evident from the mass spectrometer signal at the mass-to-charge ratio, $m/z = 46$ (HCOOH⁺) as the ice sublimates. The detection of formic acid was confirmed using isotopically labeled water-d2 with carbon monoxide, leading to formic acid-d2 (DCOOD). The temporal fits of the reactants, reaction intermediates, and products elucidate two reaction pathways to formic acid in carbon monoxide–water ices. The reaction is induced by unimolecular decomposition of water forming atomic hydrogen (H) and the hydroxyl radical (OH). The dominating pathway to formic acid (HCOOH) was found to involve addition of suprathreshold hydrogen atoms to carbon monoxide forming the formyl radical (HCO); the latter recombined with neighboring hydroxyl radicals to yield formic acid (HCOOH). To a lesser extent, hydroxyl radicals react with carbon monoxide to yield the hydroxyformyl radical (HOCO), which recombined with atomic hydrogen to produce formic acid. Similar processes are expected to produce formic acid within interstellar ices, cometary ices, and icy satellites, thus providing alternative processes for the generation of formic acid whose abundance in hot cores such as Sgr-B2 cannot be accounted for solely by gas-phase chemistry.

Key words: astrochemistry – comets: general – cosmic rays – infrared: ISM – ISM: molecules – methods: laboratory – molecular processes

Online-only material: color figures

1. INTRODUCTION

Formic acid (HCOOH) is the simplest organic acid and the first acid identified in the interstellar medium (ISM) by Zuckerman et al. (1971). This acid has a potential to form biologically important molecules like acetic acid (CH₃COOH) and glycine (NH₂CH₂COOH), since it shares common structural elements (Liu et al. 2001). In the gas phase, formic acid has been observed toward star-forming regions (Ikeda et al. 2001; Bisschop et al. 2007c), hot cores (Liu et al. 2001, 2002), hot corinos (Bottinelli et al. 2007), the galactic center cloud (Requena-Torres et al. 2006), and cold dark clouds (Irvine et al. 1990; Turner et al. 1999; Requena-Torres et al. 2007). Bockelée-Morvan et al. (2000) reported the first detection of formic acid in a cometary coma (Hale–Bopp) and calculated its abundance to be about 0.09% relative to water. Formic acid in the solid state on interstellar grains has also been observed in both low- and high-mass star-forming regions (Schutte et al. 1999; Keane et al. 2001; Gibb et al. 2004). The abundance of the observed solid formic acid is a factor of 10⁴ higher than that of gaseous formic acid in high-mass star-forming regions (Bisschop et al. 2007c, 2007a). Recent observations obtained with the *Spitzer* surveys of low-mass Young Stellar Objects (YSOs) have provided that formic acid column densities are 1%–5% with respect to solid water (Boogert et al. 2008).

Both gas-phase reactions and grain-surface processes have been suggested to produce interstellar formic acid (Liu et al.

2001). Although formic acid formation in the gas phase is yet to be investigated experimentally (Irvine et al. 1990; Lattanzi et al. 2008; Vignen et al. 2010), grain chemistry during the cold phase of star formation is a plausible source for its formation, since solid formic acid has been detected in star-forming regions and dense molecular clouds. Liu et al. (2001) proposed that observed formic acid in the galactic hot molecular cores was produced via grain chemistry, and it will be released into the gas phase by mantle sublimation. Bisschop et al. (2007a) suggested that cosmic-ray-induced desorption from the solid state may alone be enough to explain the observed gas-phase abundances of formic acid in high-mass star-forming regions.

Based on their high interstellar abundances, water and carbon monoxide are the most likely sources of interstellar formic acid. Energetic processing from radiation by both UV photons and energetic particles in the form of Galactic Cosmic Rays (GCRs) is known to be a key process that shapes the chemical evolution of interstellar environments. The UV radiation in diffuse interstellar matter is estimated to be $\phi = \sim 8 \times 10^7$ photons cm⁻² s⁻¹ (Mathis et al. 1983). Even though UV photons cannot penetrate deep into dense molecular ices, the interaction of high-energy cosmic rays with hydrogen generates an internal UV field, with a fluence estimated to be $\phi = 10^3$ photons cm⁻² s⁻¹ (Prasad & Tarafdar 1983). Following photolysis of ice mixtures containing water and carbon monoxide, the formation of formic acid has been confirmed as well as other various products, e.g., formyl radical (HCO), carbon dioxide (CO₂), formaldehyde (H₂CO), methanol (CH₃OH), and acetaldehyde (CH₃CHO; Allamandola et al. 1988; Schutte et al. 1999; Watanabe et al. 2007).

⁴ Author to whom any correspondence should be addressed.

⁵ Current address: Institute of Low Temperature Science, Hokkaido University, Sapporo, Hokkaido 060–0819, Japan.

GCRs consist of about $\sim 98\%$ protons and $\sim 2\%$ helium nuclei and have a distribution maximum around 1 MeV with $\phi = 10$ particles $\text{cm}^{-2} \text{s}^{-1}$ (Strazzulla & Johnson 1991). The MeV cosmic-ray particles can penetrate the entire icy grain and induce cascades of up to 10^2 suprathermal atoms (Kaiser et al. 1997; Kaiser 2002). The energy transferred to the ices is sufficient to ionize the molecules and hence to generate high-energy electrons, which may be born with kinetic energies up to a few keV (for more detailed discussions on the effects of irradiation on ices, see Johnson 1990; Spinks & Woods 1990; Kaiser et al. 1997; Kaiser 2002). They in turn generate a cascade of secondary electrons. Hudson & Moore (1999) studied 0.8 MeV proton bombardment of water–carbon monoxide ices and detected the products HCO, H₂CO, HCOOH, CH₃OH, CH₄, and CO₂ via infrared spectroscopy. They speculated that the simplest pathway to the synthesis of formic acid is given by the reaction of HCO with OH, which are formed by reactions (1) and (2). Garrod & Herbst (2006) studied the evolution of formic acid in the warm-up phase of hot molecular cores by means of a gas–grain chemical network. The authors argued that the most likely route to formic acid follows reaction (3):



Goumans et al. (2008) investigated the reaction of hydroxyl radicals with carbon monoxide on a carbonaceous surface theoretically utilizing density functional theory. They proposed that an HOCO radical intermediate was likely to be stabilized by intermolecular energy transfer to the surface, if the entrance barrier can be overcome and formic acid can be produced by subsequent reaction in a barrierless manner via recombination with a hydrogen atom (reaction (5)):



Nevertheless, no detailed kinetics studies on the formation of formic acid in low-temperature ices have been conducted. Rather than speculation on the reaction mechanism by solely taking infrared spectra of the pristine samples and at the end of the irradiation, it is imperative to collect infrared spectra during the irradiation online and in situ. This approach also provides some spectroscopic evidence for the formation of reaction intermediates and crucial information on the temporal evolution of reactants, reaction intermediates, and products. These concentrations versus time could be subsequently fit, thus following the kinetics in real time and providing solid data on the formation of formic acid upon ionizing radiation in interstellar ices. Here, we present studies of water–carbon monoxide (H₂O/CO) ices and irradiate these binary mixtures at 10 K with energetic electrons to investigate the formation of formic acid via potential radical intermediates. To support the peak assignments of the water–carbon monoxide ices, isotopically labeled water mixed sample with water-d₂ was used for the experiment.

2. EXPERIMENTAL

The water–carbon monoxide mixtures were condensed on a silver mirror inside an ultrahigh vacuum chamber (Bennett et al. 2004). A rotatable coldhead protrudes from the top of the chamber to hold the silver substrate in the center of the vessel. The temperature of the silver mirror is adjustable from 10 to 340 K by a closed-cycle helium refrigeration and resistive heating feedback system. Connected to the main chamber is an oil-free, magnetically levitated turbo molecular pump backed by a scroll pump, which supplies pressures as low as 1.8×10^{-11} Torr. Attached to the chamber is a differentially pumped electron source (Specs EQ22), which consists of a tungsten filament and an einzel lens to accelerate the electrons to 5 keV. The water–carbon monoxide gas mixture was prepared in a separate side chamber connected by a linear transfer mechanism to the main recipient. 16 mbar of distilled and repeatedly defrosted water was added to 4 mbar of carbon monoxide before being condensed onto the 10 K silver wafer for 2.5 minutes while recording a background pressure in the main chamber of 1.5×10^{-8} Torr. These ices are sampled by a Nicolet 6700 Fourier transform infrared (FTIR) spectrometer online and in situ; spectra are recorded in succession over the range 6000–400 cm^{-1} at a resolution of 2 cm^{-1} . During the entire experiment, infrared spectra were continuously recorded every 2 minutes to monitor the chemical modifications of the ice samples. Meanwhile, gaseous species may be analyzed by a Balzer QMG 420 quadrupole mass spectrometer via electron impact ionization with 100 eV electrons.

The gray line in Figure 1(a) shows an infrared spectrum of the pristine H₂O/CO ice mixture taken at 10 K; the infrared absorptions are compiled in Table 1. To calculate the column densities within our sample, a modified Lambert–Beers relationship is used (Bennett et al. 2004). For water, the column density was derived from the ν_3 fundamental band at 3663 cm^{-1} using an absorption coefficient of 2.0×10^{-16} cm molecule^{-1} (Zheng & Kaiser 2007). Here the column density was found to be $(1.1 \pm 0.1) \times 10^{17}$ molecules cm^{-2} . The column density of carbon monoxide was calculated from the ν_1 fundamental of carbon monoxide at 2141 cm^{-1} , using an absorption coefficient of 1.1×10^{-17} cm molecule^{-1} (Jiang et al. 1975). The derived column density was found to be $(1.4 \pm 0.1) \times 10^{17}$ molecules cm^{-2} indicating that the ratio of water to carbon monoxide within our ice sample is approximately (0.8 ± 0.2) : 1. Bouwman et al. (2007) reported that the band position of the CO stretching mode is altered when water is added to carbon monoxide ice; here, a second absorption at 2151 cm^{-1} appeared as shown in the inset of Figure 1 which is ascribed to CO–H₂O complex. The ratio of the second CO absorption/total integrated CO absorption intensity can be a tracer of the amount of CO that is mixed into the laboratory water ice. The ratio of 2151 $\text{cm}^{-1}/(2141 \text{ cm}^{-1} + 2151 \text{ cm}^{-1})$ is ~ 0.23 in the present study. Based on the densities—CO: 1.03 g cm^{-3} , H₂O: 0.93 g cm^{-3} —the equivalent thicknesses of the H₂O and CO were found to be 40 ± 4 and 64 ± 5 nm, respectively (Jamieson et al. 2006; Jenniskens et al. 1998).

The D₂O/CO ice mixture was prepared in a similar manner. The gray line in Figure 1(b) shows an infrared spectrum of the pristine D₂O/CO ice mixture taken at 10 K; the infrared absorptions are compiled in Table 2. Note that the absorption band at around 1516 cm^{-1} has previously been assigned as the ν_2 bending mode of a D-water molecule of HDO in D₂O ice at 1510 cm^{-1} (Ritzhaupt et al. 1980). The column densities were

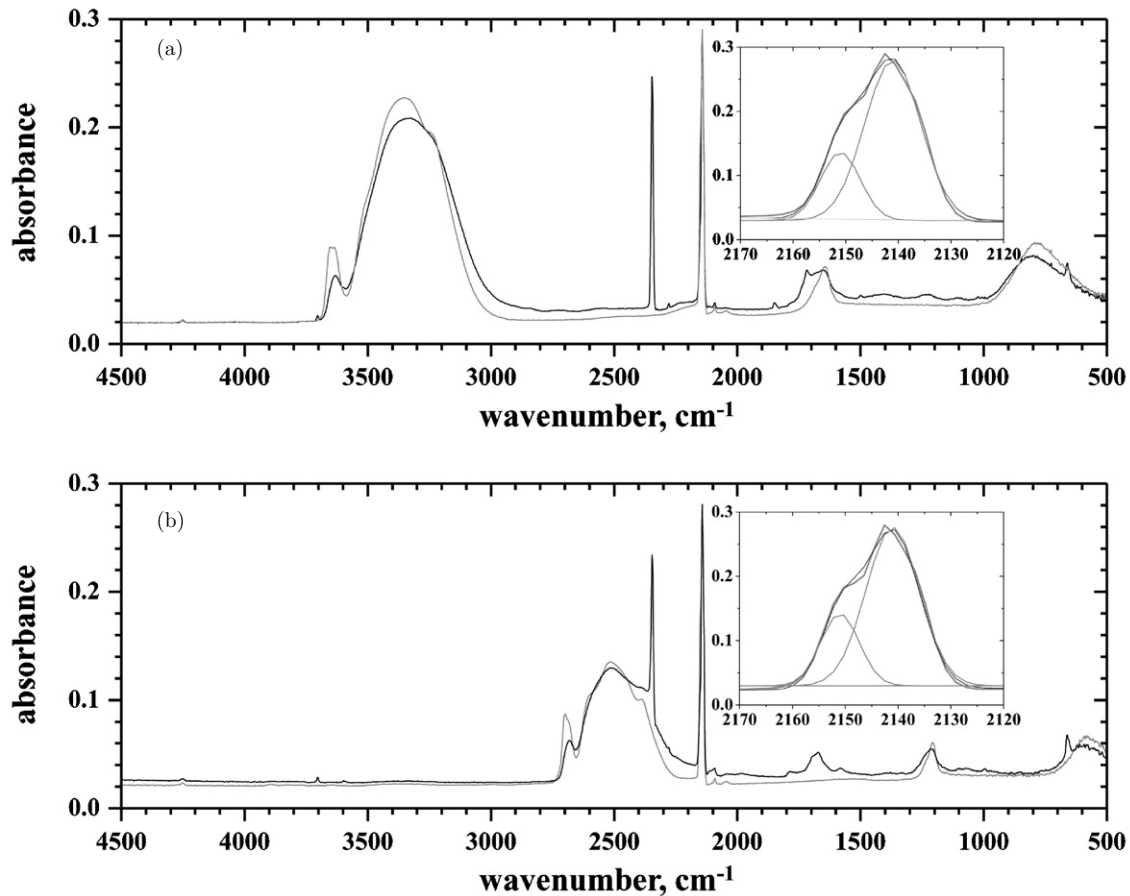


Figure 1. Complete infrared spectra over the range of 4500–500 cm^{-1} of the (a) $\text{H}_2\text{O}:\text{CO}$ ice and (b) $\text{D}_2\text{O}:\text{CO}$ ice held at 10 K prior (gray) and after the irradiation (black). The inset shows the deconvoluted regions of 2120–2170 cm^{-1} . The Gaussian fits on a linear baseline have been overlaid to aid the eye.

Table 1
Infrared Absorptions of the Water and Carbon Monoxide Ice Mixture at 10 K along with the Assignments of the Observed Bands.

Band Position (cm^{-1})	Literature Value (cm^{-1})	Assignment	Characterization
4251	4251 ^a	$2\nu_1$ CO	Overtone
3652	3655 ^b	Free H_2O^f	Fundamental
3356	3367 ^c	ν_1 out-of-phase H_2O^g	Fundamental
		ν_3 longitudinal H_2O^g	
3238	3253 ^c	ν_1 in-phase H_2O^g	Fundamental
		ν_3 transversal, H_2O^g	
2151	2148 ^b	ν_1 CO	Fundamental
2141	2138 ^b	ν_1 CO	Fundamental
2095	2091 ^a	ν_1 ^{13}CO	Isotope peak
2090	2088 ^a	ν_1 C^{18}O	Isotope peak
2047	2040 ^d	ν_1 $^{13}\text{C}^{18}\text{O}$	Fundamental
1645	1660 ^e	ν_2 H_2O	Fundamental
782	760 ^e	ν_L H_2O	Lattice mode

Notes. Tentative assignments are shown in italics.

^a Jamieson et al. (2006) and references therein.

^b Bouwman et al. (2007).

^c Mastrapa et al. (2009).

^d Bennett et al. (2009b).

^e Gerakines et al. (1995).

^f Free OH stretch from surface water molecules.

^g Zheng et al. (2006).

calculated to be $(1.1 \pm 0.1) \times 10^{17}$ molecules cm^{-2} for D_2O and $(1.4 \pm 0.3) \times 10^{17}$ molecules cm^{-2} for CO based on the reported infrared absorption and the optical constants (Bergren et al. 1978; Zheng et al. 2007). This translates into a deuterated water–carbon monoxide ratio of about $(0.8 \pm 0.3):1$, and the

ratio of $2151 \text{ cm}^{-1}/(2141 \text{ cm}^{-1} + 2151 \text{ cm}^{-1})$ is ~ 0.25 . The equivalent thicknesses of the D_2O and CO were found to be 33 ± 3 and 63 ± 14 nm, respectively.

All ices were prepared at 10 K prior to an irradiation with 5 keV electrons for 1 hr at an electron current of 100 nA. Note

Table 2
Infrared Absorptions of the Water-d2 and Carbon Monoxide Ice Mixture at 10 K along with the Assignments of the Observed Bands.

Band Position (cm ⁻¹)	Literature Value (cm ⁻¹)	Assignment	Characterization
4252	4251 ^a	2ν ₁ CO	Overtone
2700	2730 ^b	Free D ₂ O ^g	Fundamental
2520	2510 ^b	ν ₁ out-of-phase D ₂ O ^h ν ₃ longitudinal D ₂ O ^h ν ₁ in-phase D ₂ O ^h ν ₃ transversal, D ₂ O ^h	Fundamental
2149	2148 ^c	ν ₁ CO	Fundamental
2141	2138 ^c	ν ₁ CO	Fundamental
2095	2091 ^a	ν ₁ ¹³ C O	Isotope peak
2090	2088 ^a	ν ₁ C ¹⁸ O	Isotope peak
2044	2040 ^d	ν ₁ ¹³ C ¹⁸ O	<i>Fundamental</i>
1516	1510 ^e	ν ₂ HDO	Fundamental
1207	1212 ^f	ν ₂ D ₂ O	Fundamental
586	605 ^f	ν _L D ₂ O	Lattice mode

Notes. Tentative assignments are shown in italics.

^a Jamieson et al. (2006) and references therein.

^b Kizhakevariam et al. (1995) and references therein.

^c Bouwman et al. (2007) and references therein.

^d Bennett et al. (2009b).

^e Ritzhaupt et al. (1980).

^f Ockman (1958).

^g Free OD stretch from surface-deuterated water molecules.

^h Zheng et al. (2007).

that the electron beam covers an area of 3.2 ± 0.3 cm², and that the extraction efficiency of the electron gun is quoted as 78.8% by the manufacturer. A Monte Carlo simulation (CASINO) was used to model the electron trajectory in this ice mixture. From this simulation, the linear energy transfer (LET) to the sample was calculated to be 3.8 ± 0.1 keV μm⁻¹, corresponding to an average dose of 1.4 ± 0.2 eV per molecule (Hovington et al. 1997). The ices were irradiated at 10 K with 5 keV electrons generated in an electron gun by scanning the electron beam over an area of 3.2 ± 0.3 cm². Accounting for the extraction efficiency of 78.8% of the electrons, the target is exposed to 1.8×10^{15} electrons over an irradiation time of 60 minutes. Since more than 99.9% of the energy loss of MeV protons is through inelastic electronic interactions (S_e) within the target medium, which are simulated directly with our keV electrons, the extent of chemical modification occurring within our ices is expected to be dependant only on the LET (see Bennett et al. 2009a for further details). After scaling for the difference in the electronic LET in our experiments (3.8 keV μm⁻¹) to the actual cosmic-ray energy deposition of a 1 MeV proton (4.23 keV μm⁻¹), we can conclude that 1 s of our laboratory experiments simulates the processing of interstellar ices over $(1.7 \pm 0.2) \times 10^{11}$ s. Therefore, our laboratory experiments mimic a timescale of about $2.0 \pm 0.2 \times 10^7$ yr (a typical lifetime of an interstellar cloud). To ensure that all the reaction products were stable, the samples were kept under isothermal conditions for 1 hr. Afterward, the ice samples were warmed slowly (0.5 K minute⁻¹) from 10 to 300 K. A blank experiment was conducted in a similar way as the actual experiments, but without exposing the samples to the electron beam.

3. RESULTS

3.1. Infrared Band Assignment

After the sample was irradiated for 1 hr with 5 keV electrons at a current of 100 nA, the spectrum shows several new

absorption bands (Figures 1(a) and (b), black line), summarized in Tables 3 and 4 for H₂O/CO and D₂O/CO binary ice mixtures, respectively. Carbon dioxide (CO₂) was readily observed once the irradiation started as evident by its intense ν₃ absorption at 2345 cm⁻¹. Other assignments for carbon dioxide included 3703 (ν₁+ν₃), 3600 (2ν₂+ν₃), 678 and 661 cm⁻¹ (ν₂), as well as the ν₃ vibration of the ¹³C isotope of carbon dioxide identified at 2278 cm⁻¹ and of the OC¹⁸O isotope found at 2327 cm⁻¹. These values are in close agreement with the assignments given by Gerakines et al. (1995) and our previous works (Jamieson et al. 2006; Zheng & Kaiser 2007; Bennett et al. 2009a and 2009b). A band centered at 1274 cm⁻¹ could also be assigned to carbon dioxide (see the inset of Figure 2). This weak feature results from a splitting of the nearly degenerate ν₁ and 2ν₂ bands, an effect called Fermi resonance. There exist similar orbital symmetry elements that are common to both vibrations and, therefore, mixing of these bands is forbidden by perturbation theory. This gives rise to two distortion frequencies, ν₊ = 1383 cm⁻¹ and ν₋ = 1276 cm⁻¹, as studied by Falk (1987) and Gale et al. (1985). Both features were also observed by our lab in previous experiments with carbon dioxide ice, but only the lower energy band was observed in the current study. Carbon dioxide production was also confirmed during irradiation of the D₂O/CO ice mixture as shown in Figure 1(b), Figure 3, and Table 4.

Formaldehyde (H₂CO) can be identified via three of its fundamentals: the ν₅ (CH₂ rocking) at 1250 cm⁻¹ and ν₃ (CH₂ scissoring) at 1499 cm⁻¹ as shown in Figure 2. Formaldehyde has a strong absorption at 1718 cm⁻¹ (ν₂, CO stretching), we can clearly see a strong absorption around 1710 cm⁻¹. However, this band could not be uniquely identified due to strong overlap mainly due to formic acid and water, which were also observed over the 1600–1800 cm⁻¹ region. These bands were also identified by Gerakines et al. (1996) at 1244, 1497, and 1719 cm⁻¹ as well as by Hudson & Moore (2000) at 1248, 1499, and 1712 cm⁻¹. These absorptions are found to be in good agreement with polycrystalline formaldehyde at 4 K,

Table 3
Observed Peak Positions and Assignments of New Products in the Irradiated Water–Carbon Monoxide Ices.

Band Position (cm ⁻¹)	Literature Position (cm ⁻¹)	Assignment	Characterization
3703	3707 ^a	$\nu_1 + \nu_3$ CO ₂	Combination
3600	3602 ^a	$2\nu_2 + \nu_3$ CO ₂	Combination
2345	2346 ^a	ν_3 CO ₂	Fundamental
2327	2330 ^a	ν_3 OC ¹⁸ O	Isotope peak
2278	2281 ^a	ν_3 ¹³ CO ₂	Isotope peak
<i>2114</i>	<i>2112^a</i>	ν_1 CO-Ag	<i>Fundamental</i>
1852	1853 ^b	ν_3 HCO	Fundamental
1847	1848 ^c	ν_2 <i>trans</i> -HOCO	Fundamental
1839	1833 ^d	ν_2 <i>trans</i> -HOCO	Fundamental
1785	1797 ^d	ν_2 <i>cis</i> -HOCO	Fundamental
1718	1726 ^e	ν_2 H ₂ CO	Fundamental
1690	1705, 1685 ^f	ν_3 HCOOH	Fundamental
1499	1496 ^e	ν_3 H ₂ CO	Fundamental
<i>1358</i>	<i>1384, 1353^g</i>	ν_2 HCOO ⁻	<i>Fundamental</i>
1274	1273 ^a	$2\nu_2$ CO ₂	Overtone
1250	1245 ^e	ν_5 H ₂ CO	Fundamental
1224	1227 ^h	ν_6 HCOOH	Fundamental
1175	1171 ⁱ	ν_6 H ₂ CO	Fundamental
1095	1092 ^b	ν_2 HCO	Fundamental
1023	1041, 1031 ^e	ν_8 CH ₃ OH	Fundamental
678	677 ^j	ν_2 CO ₂	Fundamental
661	660 ^j	ν_2 CO ₂	Fundamental

Notes. Tentative assignments are shown in italics.

^a Jamieson et al. (2006) and references therein.

^b Bennett & Kaiser (2007).

^c Forney et al. (2003).

^d Milligan & Jacox (1971).

^e Bennett et al. (2007).

^f Watanabe et al. (2007).

^g Hudson & Moore (2000).

^h Bisschop et al. (2007a).

ⁱ Tso & Lee (1984).

^j Zheng & Kaiser (2007).

where they appear at 1250, 1494, and 1715 cm⁻¹ reported by Harvey & Ogilvie (1962).

Deuterated formaldehyde (D₂CO) was also identified from irradiated D₂O/CO ice mixtures: the ν_5 (CD₂ rocking) at 997 cm⁻¹ and ν_3 (CD₂ scissoring) at 1102 cm⁻¹, ν_2 (CO stretching) at 1670 and 1695 cm⁻¹ as shown in Figure 3 and Table 4. Hidaka et al. (2007) performed experiments on thermalized (50–100 K) deuterium atom exposure of CO-capped water ice at 10–20 K and observed D₂CO identified at 991, 1103, and 1677 cm⁻¹. Tso & Lee (1984) studied IR absorption frequencies of D₂CO molecules isolated in an oxygen matrix and identified dimer absorptions at 1688 cm⁻¹ as well as the monomer absorptions at 1695 cm⁻¹. Therefore, the absorption at 1670 cm⁻¹ on the low-frequency side may be derived from dimer absorption of D₂CO in the binary mixed ice, shifted slightly due to a difference in our ice composition.

Formic acid (HCOOH) was found via its ν_3 band (C = O stretch) at around 1690 cm⁻¹, and ν_6 band (C–O stretch) at 1224 cm⁻¹ (Table 3; Figure 2). These values compare nicely with previously reported peak positions for HCOOH bands for the tertiary HCOOH:H₂O:CO ice mixture at 15 K, where these absorptions appeared at 1705 and 1227 cm⁻¹, respectively (Bisschop et al. 2007a). Watanabe et al. (2007) identified HCOOH at 1705 and 1220 cm⁻¹ after photolysis of the H₂O–CO mixed ice layers. Hudson & Moore (1999) studied 0.8 MeV proton bombardment of H₂O–CO ice and identified the product HCOOH at 1219 cm⁻¹.

The isotopically labeled formic acid, DCOOD, was found via its ν_3 (C = O stretch) at around 1735 cm⁻¹. Milligan & Jacox (1971) previously identified DCOOD at 1726 cm⁻¹ after vacuum-ultraviolet photolysis of D₂O in a CO matrix at 14 K. Tso & Lee (1984) observed IR absorption frequencies of DCOOD molecules isolated in a neon matrix also at 1726 cm⁻¹. Two weak, broad absorptions at around 1395 and 1333 cm⁻¹ are in fair agreement with the $2\nu_5$ (OD bending) and $2\nu_7$ (OCO deformation) bands observed at 1419 and 1327 cm⁻¹ for polycrystalline DCOOD at 6 K (Zelmann et al. 1975). However, it should be noted that these bands were not observed in several other infrared studies of pure DCOOD ice (Millikan & Pitzer 1958) and matrix isolated DCOOD (Milligan & Jacox 1971; Tso & Lee 1984).

The formyl radical (HCO) was identified via its ν_3 (C = O stretching) absorption mode at 1852 cm⁻¹. The weak peak at 1095 cm⁻¹ can also be attributable to the ν_2 (HCO bending) absorption mode of HCO. These band positions are in good agreement with our previous identification of HCO in CH₄ and CO₂ binary ices at 1853 cm⁻¹ and 1092 cm⁻¹ (Bennett & Kaiser 2007). These bands disappeared after heating at 40 K. This behavior verifies the assignment of these absorptions to highly reactive species such as radicals. Therefore, the temperature behavior of these bands support the fact that they are associated with the formyl radical. Hudson & Moore (2000) reported this molecule at 1848 cm⁻¹.

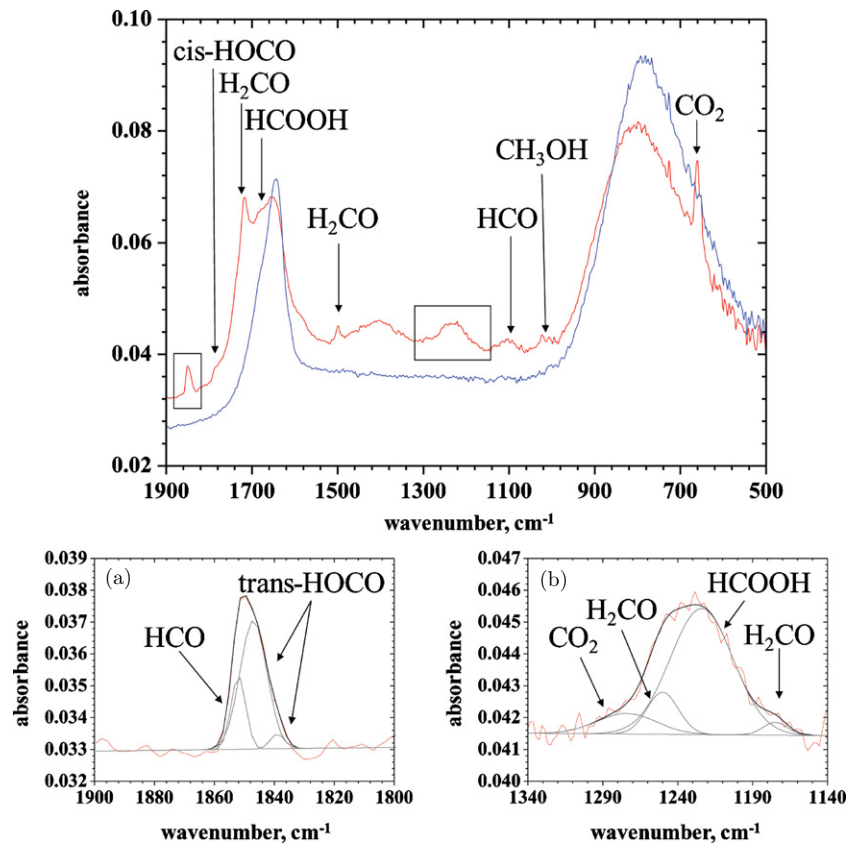


Figure 2. Infrared spectra over the range of 1900–500 cm^{-1} of the water–carbon monoxide ice held at 10 K prior (blue) and after the irradiation (red). Insets show the deconvoluted regions of 1800–1900 cm^{-1} and 1140–1340 cm^{-1} . The Gaussian fits on a linear baseline have been overlaid to aid the eye. (A color version of this figure is available in the online journal.)

Table 4

Observed Peak Positions and Assignments of New Products in the Irradiated Water-d₂–Carbon Monoxide Ices.

Band Position (cm^{-1})	Literature Position (cm^{-1})	Assignment	Characterization
3703	3707	$\nu_1 + \nu_3$ CO ₂	Combination
3597	3602 ^a	$2\nu_2 + \nu_3$ CO ₂	Combination
2346	2346 ^a	ν_3 CO ₂	Fundamental
2328	2330 ^a	ν_3 OC ¹⁸ O	Isotope peak
2280	2281 ^a	ν_3 ¹³ CO ₂	Isotope peak
2114	2112 ^a	ν_1 CO-Ag	<i>Fundamental</i>
1984	1981 ^a	ν_1 C ₂ O	Fundamental
1789	1811, 1825 ^b	ν_2 <i>trans</i> -DOCO	Fundamental
1773	1798 ^b	ν_2 <i>cis</i> -DOCO	Fundamental
1735	1726 ^b	ν_3 DCOOD	Fundamental
1695	1695 ^c	ν_2 D ₂ CO	Fundamental
1670	1677 ^d	ν_2 D ₂ CO	Fundamental
1645	1625 ^e	ν_5 DCOO ⁻	Fundamental
1582	1589 ^c	ν_5 DCOO ⁻	Fundamental
1395	1419 ^f	$2\nu_5$ DCOOD	<i>Overtone</i>
1333	1327 ^f	$2\nu_7$ DCOOD	<i>Overtone</i>
1102	1103 ^c	ν_3 D ₂ CO	Fundamental
1072	1067 ^d	ν_6 CD ₃ OD	Fundamental
997	989 ^c	ν_5 D ₂ CO	Fundamental
852	853 ^b	ν_2 DCO	Fundamental
662	660 ^g	ν_2 CO ₂	Fundamental

Notes. Tentative assignments are in italics.

^a Jamieson et al. (2006) and references therein.

^b Milligan & Jacox (1971).

^c Tso & Lee (1984).

^d Hidaka et al. (2007).

^e Forney et al. (2003).

^f Zelsmann et al. (1975).

^g Zheng & Kaiser (2007).

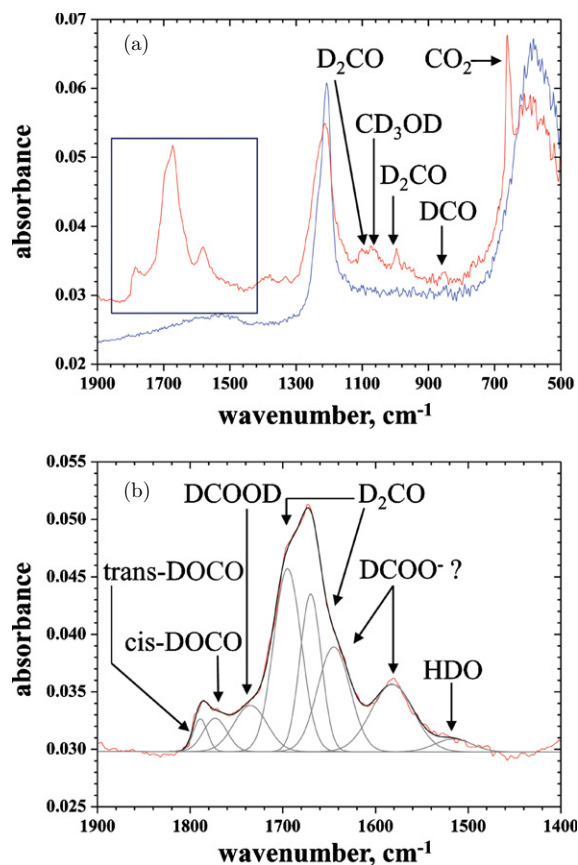


Figure 3. Infrared spectra over the range of (a) 1900–500 cm^{-1} of the water-d₂-carbon monoxide ice held at 10 K prior (blue) and after the irradiation (red), and (b) the deconvoluted region of 1400–1900 cm^{-1} . The Gaussian fits on a linear baseline have been overlaid to aid the eye.

(A color version of this figure is available in the online journal.)

The isotopically labeled formyl radical, DCO, was identified via its ν_2 (DCO bending) absorption mode at 853 cm^{-1} (Figure 3). Milligan & Jacox (1971) previously identified DCO at 853 cm^{-1} after vacuum-ultraviolet photolysis of D₂O in a CO matrix at 14 K. Hidaka et al. (2007) performed experiments on thermalized (50–100 K) deuterium atom exposure of CO ice at 10–20 K. They reported that no peak derived from DCO was observed, though D₂CO and CD₃OD production was clearly confirmed.

The hydrocarboxyl radical, HOCO, was detected through its ν_2 (CO stretching) absorptions at 1847 and 1839 cm^{-1} (Figure 2); this is consistent with two different matrix sites of the *trans* isomer, which has previously been identified at 1848 cm^{-1} in a neon matrix (Forney et al. 2003) and at 1833 cm^{-1} in a carbon monoxide matrix (Milligan & Jacox 1971). Our previous work also found the corresponding absorption by *trans*-HOCO at the same position in CH₄ and CO₂ binary ices, i.e., 1847 and 1839 cm^{-1} (Bennett & Kaiser 2007). The *cis* structure could be assigned to a peak at 1785 cm^{-1} shoulder (Figure 2). Milligan & Jacox (1971) identified *cis*-HOCO radicals at 1797 cm^{-1} after vacuum-ultraviolet photolysis of H₂O in a CO matrix at 14 K. Oba et al. (2010) studied surface reactions between CO and thermalized (\sim 100 K) OH radicals, produced by dissociating water molecules in microwave-induced plasma and cooled down to 100 K. They suggested that the formation of *cis*-HOCO was observed at 1774 cm^{-1} as well as CO₂ and *trans*-HOCO.

The deuterated carboxyl radical (DOCO) was detected through its ν_2 (CO stretching) absorptions at 1789 and

1773 cm^{-1} (Figure 3); similar peaks have been observed at 1811 and 1798 cm^{-1} during vacuum-ultraviolet photolysis of D₂O in a CO matrix at 14 K (Milligan & Jacox 1971). Milligan & Jacox (1971) proposed that these peaks are derived from *trans*- and *cis*-DOCO radicals, respectively. Although the peak positions differ slightly (\sim 25 cm^{-1}) from the literature (Milligan & Jacox 1971), the interval between these two peaks is quite similar (\sim 15 cm^{-1}). According to Milligan & Jacox (1971), DCO also has an absorption occurring in this region, the ν_3 mode (C = O stretching) at 1803 cm^{-1} , but the relative band strength is weaker than its strongest band, ν_2 (DCO bend), at 853 cm^{-1} . In the present work, the band strengths of the absorption bands observed around 1789 and 1773 cm^{-1} are much stronger than that at 853 cm^{-1} , suggesting that the origin of the strong absorption bands is not DCO but *trans*- and *cis*-DOCO. All peaks assumed to be *trans*- and *cis*-HOCO or DOCO radicals were found to disappear when the sample was warmed up to 40 K, which is consistent with observations by Milligan & Jacox (1971). Therefore, these peaks may be attributed to *trans*- and *cis*-HOCO or DOCO radicals.

Weak absorptions arising from the fundamental ν_8 of methanol, CH₃OH, could be found at 1023 cm^{-1} . Watanabe et al. (2007) found the absorption at 1022 cm^{-1} , and our previous work also found the corresponding absorption at 1034 cm^{-1} (Bennett et al. 2007). Deuterated methanol, CD₃OD, was also observed via its ν_6 absorption at 1072 cm^{-1} from the irradiated D₂O/CO mixed ice sample as shown in Table 4 and Figure 3. Finally, a very small absorption band was observed at around 2850 cm^{-1} . This peak can be attributed to hydrogen peroxide (H₂O₂; Zheng et al. 2006). The dicarbon monoxide molecule (C₂O) has previously been established as a product formed upon the irradiation of pure carbon monoxide ices, where it was observed at 1981 cm^{-1} (Jamieson et al. 2006). We can see a very small absorption at 1984 cm^{-1} in the irradiated D₂O/CO ice samples, presumably since the relative abundance of CO may be higher than the H₂O/CO ice samples within the margin of error bars described in Section 2. In addition, we tentatively assign the carrier of the band at 2114 cm^{-1} to carbon monoxide which is surface bound to the silver surface, as has been previously reported (Froben et al. 1996; Jamieson et al. 2006).

The present study indicated the presence of both a shoulder at around 1550–1600 cm^{-1} and a small peak at 1358 cm^{-1} in the irradiated H₂O/CO spectrum but these could not be adequately resolved for any further analysis. Hudson & Moore (2000) assigned absorptions appearing at 1589, 1384, and 1353 cm^{-1} to the formate ion, HCOO⁻. However, these frequencies are in disagreement with subsequently published matrix isolation experiments and calculated frequencies by Forney et al. (2003). Watanabe et al. (2007), on the other hand, assigned the small peak appearing at 1354 cm^{-1} to acetaldehyde, CH₃CHO, from photolysis of H₂O/CO samples. However, we cannot rule out the presence of HCOO⁻ as the observed absorptions at 1645 and 1582 cm^{-1} from the irradiated D₂O/CO sample were consistent with the ν_5 (CO₂ stretching) for the deuterated formate ion, DCOO⁻, from Na⁺D(CO₂) and Ne matrix at 1625 and 1589 cm^{-1} reported by Forney et al. (2003), respectively.

3.2. Mass Spectrometry

3.2.1. H₂O/CO Ice

During the electron exposure at 10 K, no species were detected in the gas phase with the exception of a trace amount of hydrogen gas ($m/z = 2$; H₂⁺), able to be released from the

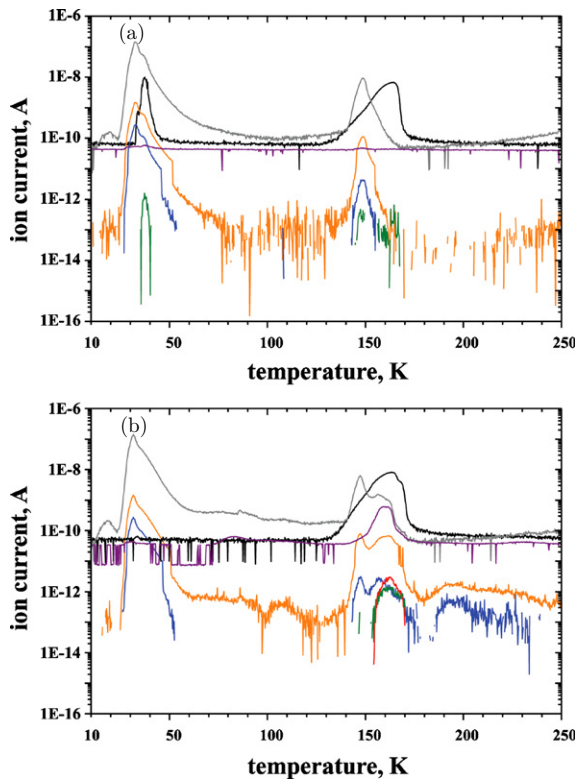


Figure 4. Evolution of the ion currents of $m/z = 18$ (H_2O^+ ; black), 28 (CO^+ ; gray), 29 ($^{13}\text{CO}^+/\text{HCO}^+$; orange), 30 ($\text{C}^{18}\text{O}^+/\text{H}_2\text{CO}^+$; blue), 32 ($\text{O}_2^+/\text{CH}_3\text{OH}^+$; green), 44 (CO_2^+ ; purple), and 46 (HCOOH^+ ; red) during the warm-up of the samples irradiated at (a) 0 nA (blank) and (b) 100 nA.

(A color version of this figure is available in the online journal.)

ice even at such low temperatures. After the electron exposure, the $\text{H}_2\text{O}/\text{CO}$ ice samples were kept isothermally at 10 K for 1 hr and were then warmed up with a heating rate of $0.5 \text{ K minute}^{-1}$. Figure 4 depicts the ion currents of water ($m/z = 18$; H_2O^+), carbon monoxide ($m/z = 28$; CO^+), formyl radical or ^{13}C isotope of carbon monoxide ($m/z = 29$; HCO^+ or $^{13}\text{CO}^+$), formaldehyde or ^{18}O isotope of carbon monoxide ($m/z = 30$; H_2CO^+ or C^{18}O^+), methanol or the oxygen molecule ($m/z = 32$; CH_3OH^+ or O_2^+), carbon dioxide ($m/z = 44$; CO_2^+), and formic acid ($m/z = 46$; HCOOH^+) during the warm-up phases of (a) the blank run and (b) the irradiation experiments at 100 nA versus the temperature.

First, it is crucial to comment on the blank experiment (Figure 4(a)). Most importantly, no $m/z = 46$ (formic acid, HCOOH^+) was observed in the blank experiment. The first molecule to sublime was carbon monoxide ($m/z = 28$; CO^+). Bennett et al. (2009b) previously reported that carbon monoxide and its isotopomers sublime within the range of 24–44 K peaking at around 35 K. Previous studies have also demonstrated that while bulk carbon monoxide has a desorption peak at 24 K (Collings et al. 2003a), it is seen to desorb over the range of 20–60 K when co-condensed with water (Collings et al. 2003b). In the present study, the two broad peaks for carbon monoxide ($m/z = 28$; CO^+) were observed at around 20 and 32 K. In the case of the peak at ~ 20 K, it is likely to be from weakly bound surface molecules. The ^{13}C isotope of carbon monoxide ($m/z = 29$; $^{13}\text{CO}^+$) and the ^{18}O isotope of carbon monoxide ($m/z = 30$; C^{18}O^+) also sublimated between 25 and 50 K where the peak desorption temperature was observed at 32 K, which is also good agreement. It should be noted that water ($m/z = 18$; H_2O^+) which adsorbed on the ice surface also partially co-

sublimates as carbon monoxide sublimates between 30 and 45 K with a maximum signal at around 38 K.

When the temperature reaches 140 K, water ($m/z = 18$; H_2O^+) starts to undergo a phase change and also sublime as reported by Zheng et al. (2006). Carbon monoxide ($m/z = 28$; CO^+) and its isotopomers ($m/z = 29$; $^{13}\text{CO}^+$ and $m/z = 30$; C^{18}O^+) were also observed together with water desorption, suggesting that these molecules were trapped within the bulk water ice and failed to sublime completely between 20 and 50 K. Collings et al. (2003b) previously reported carbon monoxide sublimation trapped within water ice desorbing in two separate events as the ice undergoes a phase change at 140 K and sublimates at 160 K; note that due to our increased heating rate these events are converged.

It should be noted that molecular oxygen ($m/z = 32$; O_2^+) observed between 35–40 K and 140–150 K could originate from the fragmentation of the desorbed water molecule due to the electron impact ionizer of the mass spectrometric detector as shown in our previous publication on electron irradiation of pure H_2O ice (Zheng et al. 2006). In fact, neither water ($m/z = 18$) nor molecular oxygen ($m/z = 32$) could be observed through mass spectrometry over the range 35–40 K in the irradiated samples as shown in Figure 4(b). In addition, we should keep in mind that ion–molecule reactions occurring in the mass spectrometer ionization region can generate small amounts of HCO^+ ($m/z = 29$), H_2CO ($m/z = 30$), and CH_3OH ($m/z = 32$), which can contribute to the observed signals. At 140 K, we begin to observe the sublimation of water, accompanied by some additional carbon monoxide being released.

We next discuss the mass spectra obtained from the irradiated sample (Figure 4(b)). As the sample is warmed up, carbon dioxide ($m/z = 44$; CO_2^+) starts to sublime, where the two broad peaks were observed at around 85 K and 150 K. In the latter case, carbon dioxide is co-desorbed with water desorption, again due to the trapping of this molecules within the water matrix. Comparison to the blank experiments indicates that this species is definitely produced within our ices and not contamination from the walls of our vacuum chamber. We can clearly see that the formic acid ($m/z = 46$; HCOOH^+) begins to sublime at around 155 K. In addition, the $m/z = 29$ (HCO^+) signal was increased as formic acid sublimated from the mixed ice sample, due to the fragmentation of desorbed HCOOH by the electron impact ionizer of the mass spectrometric detector—similar behavior was obtained from temperature programmed desorption of formic acid with solid water deposited on tungsten at 80 K by Bahr et al. (2005).

A peak at $m/z = 30$ appeared at about 157 K indicating the presence of H_2CO formation rather than the ^{18}O isotope of carbon monoxide ($m/z = 30$; C^{18}O^+), since this peak was not observed in the blank experiment. Madzunkov et al. (2009) performed 3 eV beam of hydrogen atom irradiation of carbon monoxide molecules adsorbed on a gold surface at 4.8 K and analyzed the products using quadrupole mass spectrometry. The authors also assigned the $m/z = 30$ signal between 150 K and 160 K as H_2CO . The small increment of $m/z = 32$ at around 150–175 K could be attributable to methanol production, which is in fair agreement with the reported desorption temperature from water ice by Bahr et al. (2008), as detectable levels of methanol (CH_3OH) were present in the FTIR spectra.

3.2.2. $\text{D}_2\text{O}/\text{CO}$ ice

As with the non-deuterated samples, the only species observed during the irradiation of the ice was a minor amount

Table 5
Summary of Temporal Changes in Column Density of the Observed Species Based on the Indicated Band Position at the End of Irradiation, and Corresponding A-Values.

Species	Band Position (cm ⁻¹)	A (cm molecule ⁻¹)	Change in Column Density (molecules cm ⁻²) ^a
H ₂ O	3663	2.0×10^{-16} b	$-5.5 \pm 4.2 \times 10^{15}$
CO	2140	1.1×10^{-17} c	$-2.1 \pm 0.5 \times 10^{16}$
CO ₂	2342	7.6×10^{-17} d	$3.4 \pm 0.4 \times 10^{15}$
HCO	1852	1.5×10^{-17} e	$4.0 \pm 0.7 \times 10^{14}$
<i>t</i> -HOCO	1847, 1839	3.6×10^{-17} f	$3.5 \pm 0.6 \times 10^{14}$
H ₂ CO	1499	4.0×10^{-18} g	$1.5 \pm 0.4 \times 10^{15}$
HCOOH	1224	1.5×10^{-17} g	$3.7 \pm 0.9 \times 10^{15}$

Notes. The temporal profile during irradiation produced from these bands is shown for each species in Figure 6.

^a The stated error given is the standard deviation of the calculated area from Gaussians fitted to the species during the deconvolution process combined with an estimated absolute error (2% for reactants, 10% for products).

^b Zheng & Kaiser (2007).

^c Jiang et al. (1975).

^d Gerakines et al. (1995).

^e Bennett et al. (2005).

^f Bennett & Kaiser (2007).

^g Hudson & Moore (1999).

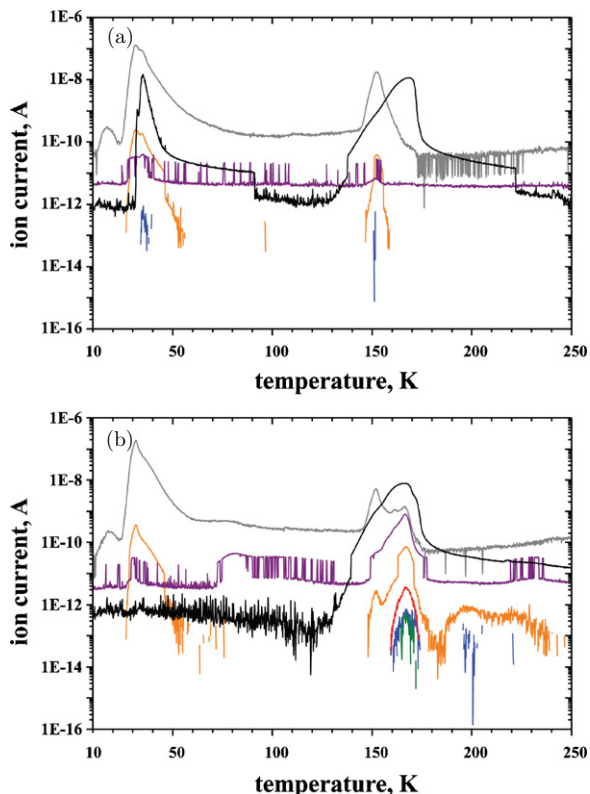


Figure 5. Evolution of the ion currents of $m/z = 20$ (D_2O^+ ; black), 28 (CO^+ ; gray), 30 ($C^{18}O/DCO^+$; orange), 32 (O_2^+/D_2CO^+ ; blue), 34 (CD_3OD^+ ; green), 44 (CO_2^+ purple), and 48 ($DCOOD^+$; red) during the warm-up of the samples irradiated at (a) 0 nA (blank) and (b) 100 nA.

(A color version of this figure is available in the online journal.)

of deuterated hydrogen ($m/z = 4$; D_2^+). The D_2O/CO ice samples were also warmed up after the electron exposure in the same manner. Figures 5(a) and (b) depict the ion currents of deuterated water ($m/z = 20$; D_2O^+), carbon monoxide ($m/z = 28$; CO^+), deuterated formyl radical or ^{18}O isotope of carbon monoxide ($m/z = 30$; DCO^+ or $C^{18}O^+$), deuterated formaldehyde or oxygen molecule ($m/z = 32$; D_2CO^+ or O_2^+), deuterated methanol ($m/z = 36$; CD_3OD^+), carbon dioxide ($m/z = 44$; CO_2^+), and deuterated formic acid ($m/z = 48$; $DCOOD^+$) during the warm-

up phases of (a) the blank run and (b) the irradiation experiments at 100 nA versus the temperature. The blank experiment of the D_2O/CO ice mixture (Figure 5(a)) shows no deuterated formic acid ($m/z = 48$; $DCOOD^+$) signals, which is consistent with the blank experiment in the H_2O/CO ice mixture (Figure 4(a)). We can see that carbon monoxide ($m/z = 28$; CO^+) starts to sublime with two broad peaks at 20 and 32 K; the ^{18}O isotope of carbon monoxide ($m/z = 30$; $C^{18}O^+$) is also observed at this time. Following carbon monoxide desorption, deuterated water ($m/z = 20$; D_2O^+) adsorbed on the ice surface also started to sublime between 30 and 45 K. Small $m/z = 32$ and $m/z = 44$ signals were observed between 30 and 40 K, which could be attributed to the oxygen molecule and carbon dioxide, respectively (Zheng et al. 2007). Deuterated water ($m/z = 20$; D_2O^+) starts to sublime again as the temperature reaches 140 K as reported by Zheng et al. (2007). Carbon monoxide and the isotopomer ($m/z = 28$, CO^+ and $m/z = 30$, $C^{18}O^+$) were also observed together with water desorption. These results are similar to those from H_2O/CO mixed ice blank experiment. Note that the $m/z = 30$ signal could be attributable to DCO formed via ion–molecule reactions occurring in the mass spectrometer. As the irradiated D_2O/CO sample is warmed up (Figure 5(b)), the carbon dioxide ($m/z = 44$; CO_2^+) and the deuterated formic acid ($m/z = 48$; $DCOOD^+$) begin to sublime in a similar way to the irradiated H_2O/CO sample as shown in Figures 4(b) and 5(b). The increased $m/z = 30$ signal between 160 and 175 K could again be due to the DCO^+ generated via the fragmentation of $DCOOD$ as we see in H_2O/CO mixed ice. Deuterated formaldehyde and methanol formations can be observed from the $m/z = 32$ (D_2CO^+) and $m/z = 36$ (CD_3OD^+) signals at around 150–175 K, consistent with the FTIR results (Table 4 and Figure 3).

4. DISCUSSION

In order to elucidate which reactions are occurring within our ices, the temporal column densities for each of the observed species were first produced using the information summarized in Table 5; the reaction schemes which were subsequently fit to these profiles are shown in Table 6. We therefore present results of these reaction schemes to demonstrate how individual reactions can be substituted or removed from these schemes, while others are found to be essential or dominant. The underlying

Table 6

Compilation of Essential Reactions along with their Derived Rate Constants within the Context of Each Reaction Scheme Investigated (See the Text for Details).

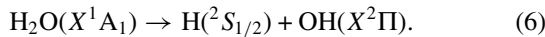
Reaction	Reaction Rate ^a						
	Scheme A	Scheme A'	Scheme A''	Scheme A'''	Scheme B	Scheme C	Scheme D
H ₂ O → H + OH	1.26 × 10 ⁻⁵	1.26 × 10 ⁻⁵	1.26 × 10 ⁻⁵	1.26 × 10 ⁻⁵	1.32 × 10 ⁻⁵	1.24 × 10 ⁻⁵	1.35 × 10 ⁻⁵
H ₂ O → 2H + O	6.88 × 10 ⁻⁶	6.88 × 10 ⁻⁶	6.91 × 10 ⁻⁶	6.92 × 10 ⁻⁶			
CO → C + O	5.38 × 10 ⁻⁸		2.44 × 10 ⁻⁶	2.44 × 10 ⁻⁶		8.80 × 10 ⁻⁶	4.00 × 10 ⁻⁶
CO → X	2.90 × 10 ⁻⁵	2.91 × 10 ⁻⁵	2.89 × 10 ⁻⁵	2.89 × 10 ⁻⁵	2.09 × 10 ⁻⁵	2.64 × 10 ⁻⁵	2.43 × 10 ⁻⁵
CO + CO → CO ₂ + C	1.96 × 10 ⁻²³	2.04 × 10 ⁻²³			7.98 × 10 ⁻²³		3.66 × 10 ⁻²³
CO + O → CO ₂	3.60 × 10 ⁻¹⁹	3.57 × 10 ⁻¹⁹	6.31 × 10 ⁻¹⁹	6.16 × 10 ⁻¹⁹		3.64 × 10 ⁻¹⁹	2.09 × 10 ⁻¹⁹
CO + OH → CO ₂ + H				2.89 × 10 ⁻¹⁹		2.08 × 10 ⁻¹⁹	
CO + H → HCO	1.31 × 10 ⁻²⁰	1.31 × 10 ⁻²⁰	1.31 × 10 ⁻²⁰	1.30 × 10 ⁻²⁰	8.32 × 10 ⁻²¹	7.87 × 10 ⁻²¹	7.10 × 10 ⁻²¹
CO + OH → HOCO	2.86 × 10 ⁻¹⁹	2.86 × 10 ⁻¹⁹	2.71 × 10 ⁻¹⁹	2.89 × 10 ⁻¹⁹	2.01 × 10 ⁻¹⁹	4.28 × 10 ⁻¹⁷	1.19 × 10 ⁻¹⁹
HCO + H → H ₂ CO	2.20 × 10 ⁻¹⁸	2.19 × 10 ⁻¹⁸	2.19 × 10 ⁻¹⁸	2.19 × 10 ⁻¹⁸	4.79 × 10 ⁻¹⁸	3.21 × 10 ⁻¹⁸	5.24 × 10 ⁻¹⁸
HCO + OH → HCOOH	3.50 × 10 ⁻¹⁶	3.51 × 10 ⁻¹⁶	3.32 × 10 ⁻¹⁶	3.52 × 10 ⁻¹⁶	1.97 × 10 ⁻¹⁶	6.15 × 10 ⁻¹⁴	1.30 × 10 ⁻¹⁶
HOCO + H → HCOOH	7.30 × 10 ⁻¹⁹	7.29 × 10 ⁻¹⁹	7.33 × 10 ⁻¹⁹	7.38 × 10 ⁻¹⁹	1.86 × 10 ⁻¹⁸	6.45 × 10 ⁻¹⁹	7.55 × 10 ⁻¹⁹
H ₂ CO → HCO + H	1.95 × 10 ⁻⁴	1.94 × 10 ⁻⁴	1.97 × 10 ⁻⁴	1.98 × 10 ⁻⁴	3.44 × 10 ⁻⁴	2.59 × 10 ⁻⁴	1.19 × 10 ⁻³
H + CO ₂ → HOCO	5.71 × 10 ⁻²¹	5.70 × 10 ⁻²¹	7.29 × 10 ⁻²¹	8.13 × 10 ⁻²¹			
H ₂ O + C → HCO + H					4.28 × 10 ⁻²⁰	3.07 × 10 ⁻²⁰	7.99 × 10 ⁻²⁰
H ₂ O + C → H ₂ CO					3.96 × 10 ⁻²¹		
CO ₂ → CO + O					1.32 × 10 ⁻⁴		
H ₂ CO → Y						3.36 × 10 ⁻⁴	3.17 × 10 ⁻⁴

Notes. ^a Unimolecular reactions (A → B) are in units of s⁻¹; bimolecular reactions (A + B → C) are in units of cm² molecules⁻¹ s⁻¹; note that the typical units for the rate of a bimolecular reaction of cm³ molecules⁻¹ s⁻¹ are not applicable here, as our “concentrations” are presented in terms of column densities (molecules cm⁻²) rather than concentration (molecules cm⁻³).

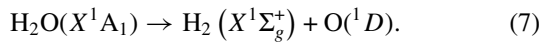
rate constants from each of these models, labeled A to D, are compiled in Table 6; the resulting kinetic fits to the column densities of each species are shown in Figure 6. In each case, the resulting system of coupled differential equations was solved numerically (Frenklach 1984; Frenklach et al. 1992, 2007).

4.1. Water

All schemes show consistent results that the unimolecular decomposition of water proceeds via rupture of a single O–H bond forming a hydrogen atom and hydroxyl radical (Equation (6)); this process is endoergic by 466 kJ mol⁻¹ (4.8 eV). This mechanism also dominates in the case of pure water samples (Zheng et al. 2006):



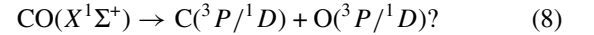
An alternative pathway has been confirmed in the gas phase and involves the generation of an excited oxygen atom and molecular hydrogen; this reaction is endoergic by 650 kJ mol⁻¹ (6.7 eV):



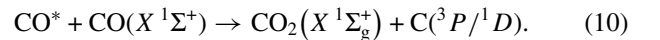
In the gas phase, only 1% and 10% of the total water degrades through this pathway when, for instance, photons of wavelength $\lambda = 146$ nm (8.5 eV) and 122 nm (10.2 eV) are used (Stief et al. 1975; Slanger & Black 1982). We included reaction (7) within scheme A (Table 6; Figure 6, red line) and found that it could be responsible for dissociating up to 35% of the total amount of water destroyed. In fact, when reaction (7) is removed from scheme A, the temporal profiles for each species (besides CO and CO₂) are poorly reproduced; however, alternative reaction pathways are included in addition to the removal of this pathway, indicating that the inclusion of this pathway is not necessarily essential to fit the data. To summarize, the decomposition of water via reaction (6) was found to be indispensable.

4.2. Carbon Monoxide

Having investigated the dissociation of the water molecule, we are turning our attention now to the carbon monoxide molecule. Can the carbon monoxide be dissociated via reaction (8),



The bond is 1071 kJ mol⁻¹ strong (11.1 eV; Bakker & Parker 2000), which is beyond the typical range of broadband hydrogen discharge lamps often used which typically extends to only 10.5 eV. Note that the lifetimes of electronically excited atoms are expected to be on the order of a few hundred milliseconds; long enough to participate in subsequent reactions (Mohammed 1990). It should be noted, however, that pure carbon monoxide ices are still processed by UV photons, whereby the initial process is thought instead to involve the electronic excitation of a molecule of carbon monoxide, which is then able to react with a neighboring carbon monoxide molecule yielding carbon dioxide and a free carbon atom (Okabe 1978):



This reaction pathway has previously been successfully incorporated into reaction networks as the sole decomposition pathway for pure carbon monoxide ices (Jamieson et al. 2006). Depending on the matrix, energetic electrons can induce a carbon–oxygen bond rupture via reaction (8) (Gerakines & Moore 2001). However, as Watanabe et al. (2007) argue, within mixed ices, the likelihood of this reaction decreases dramatically due to the decreasing likelihood of neighboring carbon dioxide molecules. Recall that the ratio of water to carbon monoxide within our ice was determined to be (0.8 ± 0.2):1, and thus, it is possible that this reaction does occur in our ices. To investigate the importance of these reactions, we removed reaction (8) to produce scheme A', and reactions (9) and (10) to produce

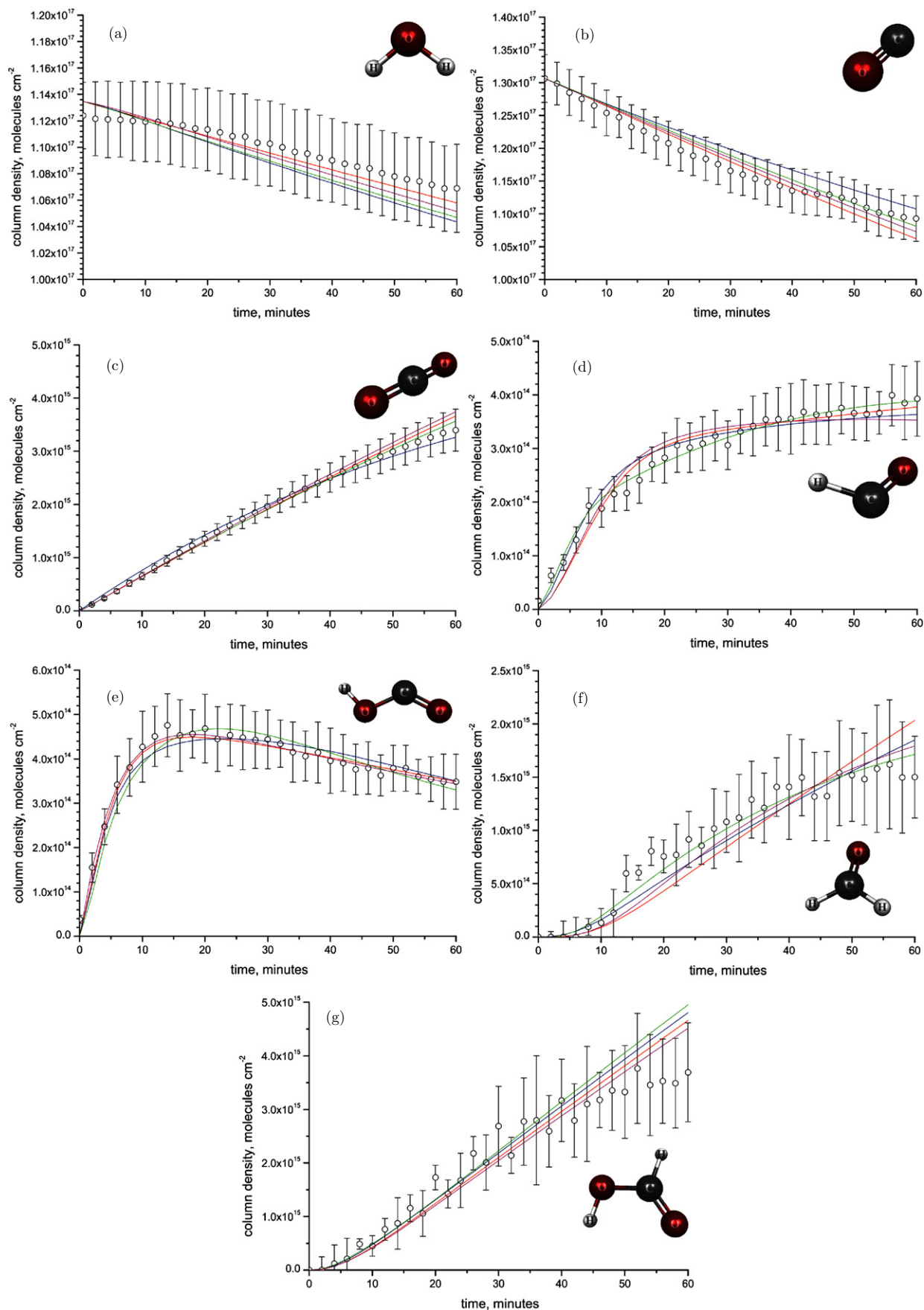
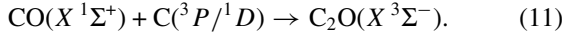


Figure 6. Temporal profiles of the column densities during the irradiation period for (a) H_2O , (b) CO , (c) CO_2 , (d) HCO , (e) *trans*- HOCO , (f) H_2CO , and (g) HCOOH . The kinetic fits are also shown for each species according to reaction schemes A (red), B (blue), C (magenta), and D (green). See the text for details. (A color version of this figure is available in the online journal.)

scheme A". Note that in both cases, the kinetic rates could be adjusted to produce identical fits (Table 6; Figure 6, red line). If both pathways are removed, the temporal profiles for CO₂, HOCO, and formic acid are not well reproduced, stressing that we must also consider the degradation of carbon monoxide. As a consequence, we expect the generation of free carbon atoms. As witnessed by Jamieson et al. (2006), these participate in the production of several linear isomers such as C₁ (l = 2, 3, 6), C_mO (m = 2–7), and C_nO₂ (n = 1, 3–5) initiated by the following process:



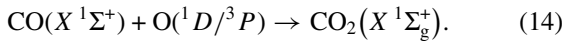
For this reason, we needed to include reaction (12) in all reaction schemes in order to account for additional miscellaneous reactions that carbon monoxide may participate in (such as the example of chain elongation reactions, as depicted in reaction (11)):



where X can be any other species not accounted for. In summary, in all schemes considered, this is the dominant destruction pathway for carbon monoxide.

4.3. Carbon Dioxide

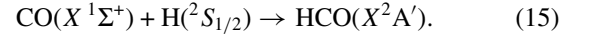
Let us next consider production mechanisms for carbon dioxide. Carbon dioxide can be formed from carbon monoxide via two reactions:



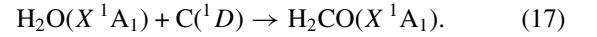
The validity of reaction (13) was investigated by Oba et al. (2010), where surface reactions of carbon monoxide held at 10 K reacted with thermal (~100 K) OH radicals produced by dissociating water molecules within microwave-induced plasma. They reported that surface reaction of carbon monoxide with hydroxyl radicals proceeded with little or no activation barrier, and the formation of carbon dioxide (as well as the formation of both *cis* and *trans* isomers of HOCO). Theoretical calculations by Song et al. (2006) indicate that the products here are exoergic by 107 kJ mol⁻¹ (1.11 eV) and that the minimum energy pathway to these products requires overcoming a barrier of 12 kJ mol⁻¹ (0.12 eV). This barrier should be accessible in our experiments since the hydroxyl radical formed in the dissociation of water is initially vibrationally excited. However, reaction (13) could not be implemented as the sole source of producing carbon dioxide in any of our reaction schemes. If reaction (14) proceeds on the triplet surface, the barrier is on the order of 25 kJ mol⁻¹ (0.26 eV), whereas the reaction is barrierless on the singlet surface (Talbi et al. 2006). Experimental evidence of this reaction comes from studies on the reactions occurring under radiolysis of mixed CO:¹⁸O₂ ices whereby the pseudo first-order generation of ¹⁸OCO carbon dioxide is readily observed (Bennett et al. 2009a). In conclusion, when reaction (14) was included in our reaction schemes, it proved to be the dominant production mechanism for producing carbon dioxide; this reaction requires a source of free oxygen atoms such as the formation via reaction (7).

4.4. Formyl Radical

The production of the formyl radical is thought to be generated primarily from the reaction of suprathreshold hydrogen atoms produced during the decomposition of water through reaction (6) with carbon monoxide:



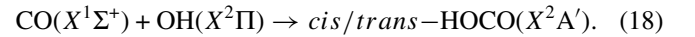
The hydrogen atoms will likely be born with excess kinetic energy, allowing them to overcome the barrier for addition of carbon monoxide of 11 kJ mol⁻¹ (0.12 eV) as calculated by Bennett et al. (2005); here, the formation of the formyl radical was also observed experimentally following the irradiation of mixed CO:CH₄ ices. However, if free carbon atoms are produced in an excited state through reactions (8)–(10), they may be able to formally insert into one or both of the sigma bonds of the water molecule, to produce both the formyl radical and formaldehyde through reactions (16) and (17), respectively:



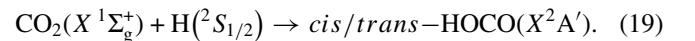
These reactions are treated within the theoretical global potential energy surface of Maeda & Ohno (2008); from their calculated energies it could be shown that reactions (16) and (17) should both be accessible after passing over an entrance barrier of 68 kJ mol⁻¹ (0.7 eV) to form a *trans*-HCOH complex prior to rearranging to the respective products, which are found to be exoergic by 180 kJ mol⁻¹ (1.9 eV) and 575 kJ mol⁻¹ (6.0 eV). Thus, we included both of these reactions into scheme B; while it was found that reaction (16) could play an important role in generating the formyl radical, reaction (17) did not substantially improve the fit for formaldehyde and was subsequently not included in further reaction schemes. To summarize, the rate constants showed that the formyl radical is predominantly produced via reaction (15).

4.5. Hydroxyformyl Radical

The hydroxyformyl radical can be formed by the recombination of hydroxyl radicals formed in reaction (6) reacting with carbon monoxide:



Here, the theoretical calculations of Song et al. (2006) indicate that the *cis* and *trans* isomers are exoergic by 92 and 100 kJ mol⁻¹ (0.95 and 1.03 eV) relative to the carbon monoxide and hydroxyl radical, respectively. Reaction (18) is in direct competition with the formation of carbon dioxide and a hydrogen atom through reaction (13). An alternative pathway to form this radical is reaction (20), i.e., the addition of a hydrogen atom to carbon dioxide:

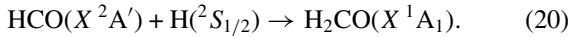


Here, the *cis* and *trans* hydroxyformyl radicals are slightly higher in energy relative to carbon dioxide and a hydrogen atom by 15 and 7 kJ mol⁻¹ (0.15 and 0.07 eV), respectively. There are also entrance barriers to form both isomers with the barrier toward forming the *cis* barrier being 114 kJ mol⁻¹ (1.18 eV) entrance barrier compared and 151 kJ mol⁻¹ (1.56 eV) to access the *trans* isomer. Once formed, it is also possible for

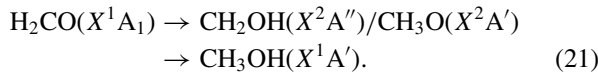
the *cis* isomer to rearrange into the *trans* isomer by overcoming a torsional rotation barrier of 27 kJ mol^{-1} (0.28 eV). Previous experiments by Bennett & Kaiser (2007) on the irradiation of $\text{CH}_4:\text{CO}_2$ ices showed the formation of *trans*-HOCO. While we included reaction (19) within scheme A, it was only accountable for a small proportion of the hydroxyformyl radical formed. When reaction (18) was removed from the reaction schemes, the profile of HOCO could not be reproduced. We therefore conclude based on the rate constants that reaction (19) is only a smaller pathway to form HOCO within our ices and that most of the HOCO is formed via reaction (18).

4.6. Formaldehyde

Formaldehyde is thought to be formed through the barrierless recombination of the formyl radical with hydrogen atoms formed through reaction (6):



This reaction has been verified to occur experimentally when CO ices are exposed to room temperature hydrogen atoms generated from a microwave-induced plasma (Watanabe et al. 2003), and when mixtures of $\text{CO}:\text{H}_2\text{O}$ ice are exposed to UV photons (Watanabe et al. 2007). In all reaction schemes, it was required for this reaction to be present, whereas its alternative production through the reaction of carbon atoms with water (reaction (17)) was shown to be dispensable. However, the profile of formaldehyde indicates that this molecular species is either being destroyed or participating within further chemistry occurring within our ice (Figure 6(f)). Thus, we included the reverse reaction of (20), which has previously been used within reaction networks (Bennett et al. 2007; Watanabe et al. 2007). It is also likely that successive hydrogenation reactions could be occurring within our ice to eventually produce methanol via the following reaction sequence:

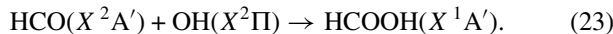


We therefore also included an additional pathway to account for the loss of formaldehyde into other chemical species not accounted for by our model (represented by Y):

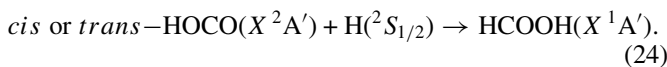


4.7. Formic Acid

Finally, let us discuss the formation mechanisms for formic acid. The first pathway we consider is given by the barrierless recombination of formyl and hydroxyl radicals, which are formed by reactions (15) and (6), respectively:



Goumans et al. (2008) proposed that HOCO on a carbonaceous surface can subsequently react in a barrierless manner with atomic hydrogen which could be formed from reaction (6):



Reactions (23) and (24) were included within all reaction schemes A to D. Consequently, we were able to extract the relative contribution of each pathway to forming formic acid. We found that in all cases, reaction (23) typically contributes

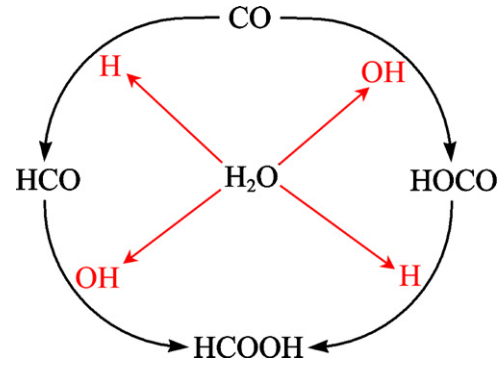


Figure 7. Summary of reaction pathways for the formation of formic acid (HCOOH) in water (H_2O)-carbon monoxide (CO) ices.

(A color version of this figure is available in the online journal.)

around 75% of the formation of formic acid, compared to 25% from reaction (24). Why does reaction (23) dominate over reaction (24)? Upon reaction with carbon monoxide, suprathreshold hydrogen atoms can easily impart their excess kinetic energy into the transition state of the reaction forming formyl, which is needed in reaction (23); in this case, the transition state is “early” on the reaction coordinate. This supports an effective incorporation of translational energy into the transition state. On the other hand, hydroxyl radicals forming HOCO in reaction (24) are not born with much excess kinetic energy due to energy and angular momentum conservation. Here, hydroxyl radicals are predominantly vibrationally excited. This vibrational excitation can easily be transferred via phonon coupling to the lattice forming thermalized hydroxyl radicals which are less reactive than vibrationally excited ones.

5. ASTROPHYSICAL IMPLICATIONS AND CONCLUSIONS

Our results indicate that formic acid (HCOOH) can be formed easily within interstellar ices subjected to ionizing radiation, if carbon monoxide and water can be found as neighboring molecules. The dominating reaction pathways are compiled in Figure 7. Carbon monoxide is typically the second most abundant molecule that is condensed on dust grains in the ISM following the water molecule (Whittet et al. 1983, 1985; Tielens et al. 1991). Carbon monoxide has been identified in both polar and apolar ice matrices toward quiescent dark clouds and YSOs of low mass, intermediate mass, and high mass (Tielens et al. 1991; Ehrenfreund et al. 1996; Gibb et al. 2004). It is known that carbon monoxide is present in two different chemical environments, i.e., polar ices dominated by water and non-polar ices where carbon monoxide is dominant with other non-polar, infrared inactive species such as nitrogen and oxygen. The amount of carbon monoxide in the solid state versus water in the solid state can be as high as 35%, which was also found to be present within polar and non-polar ices (Chiar et al. 1995; Chiar et al. 1998; Gibb et al. 2004). On the other hand, a much greater fraction of carbon monoxide ice, 40%–60% relative to water ice, was observed in regions in the Serpens dark cloud (Chiar et al. 1994), and YSOs in the Corona Australis complex, along with other sources (Chiar et al. 1998). Besides the ISM, water and carbon monoxide have also been observed in the surfaces of comets; on the surfaces of solar system bodies like Pluto and Triton (Neptune’s largest moon; Jamieson et al. 2006 and references therein; Hudson & Moore 2001), Parkinson et al. (2007) reported that carbon monoxide may be

present as well as water in the plume ejected from Enceladus, one of the Saturnian satellites. These surfaces are exposed to radiation from cosmic-ray particles, solar wind, and planetary magnetospheres. Based on our experimental data, it is likely that formic acid could be present in detectable quantities within these objects. However, it is important to keep in mind that ices in the solar system which include carbon monoxide have higher temperatures of up to 40 K than the ices in the ISM. Therefore, the formation rates of formic acid could also depend on the ice temperature.

The possibility for formic acid formation by non-energetic surface reactions has also been studied previously. For example, Garrod & Herbst (2006) investigated the formation of formic acid in the solid state without water dissociation by energetic processing. Here, hydrogen atoms from the gas phase are thought to react with adsorbed oxygen atoms on the ice surface to form the OH radical. The HCO radical could be formed in a similar manner by the reaction of gas phase hydrogen atoms with adsorbed carbon monoxide on the ice surface. Finally, when these radicals encounter one another, they could recombine to produce formic acid; however, this model could not account for the formation of formic acid at low temperatures as it requires that these radicals must be mobile on the ice surface, whereas they would not be at 10 K. However, non-equilibrium as demonstrated in our present work leading to formic acid could still be a viable production pathway. Neglecting these pathways is inconsistent with the detection of formic acid ice in cold sources such as HH 46 and background stars (Bisschop et al. 2007a) unless OH with excess energy are produced by energetic particles, e.g., cosmic-ray-induced electrons and photons. In fact, Oba et al. (2010) studied low-temperature (10 and 20 K) surface reactions of carbon monoxide with the non-energetic (~ 100 K) water fragments (H, O, OH, and H₂), which were dissociated from water molecules by microwave-induced plasma and subsequently cooled to 100 K. Their results showed that formation of formic acid is negligibly small. Bisschop et al. (2007b) studied hydrogen atom bombardment of pure carbon dioxide ice to verify that formic acid can be formed by hydrogenation of carbon dioxide ice. Hydrogen atoms, produced in a thermal-cracking device, were cooled down to ~ 300 K (~ 0.03 eV) prior to their introduction to carbon dioxide ice. They concluded that carbon dioxide does not react with thermal, atomic hydrogen at a detectable level. It is likely because of the large activation barrier to form *cis* or *trans*-HOCO from the hydrogenation of carbon dioxide, which calculated to be at least 1.1 eV. In summary, our results indicate that formic acid would be mainly synthesized via energetic processes caused by radiation of ice mantles rather than thermal surface reactions on ice mantles; consequently, formic acid can act as a tracer for energetic chemical processing of interstellar ices.

In conclusion, formic acid (HCOOH) can be efficiently synthesized when binary mixtures of water and carbon monoxide ices are irradiated with energetic electrons as generated in the track of GCR particles penetrating ices. The reaction is induced by a unimolecular decomposition of a water molecule forming atomic hydrogen (H) and the hydroxyl radical (OH). The dominating pathway to form formic acid (HCOOH) (75%) was found to involve an addition of suprathreshold hydrogen atoms to carbon monoxide forming the formyl radical (HCO); the latter recombined in the matrix cage with neighboring hydroxyl radicals to yield formic acid (HCOOH). To a minor amount (25%), hydroxyl radicals (OH) react with car-

bon monoxide to yield the hydroxyformyl radical (HOCO), which recombined with atomic hydrogen to formic acid (HCOOH).

This material is based upon work supported by the National Aeronautics Space Administration (NASA Astrobiology Institute under Cooperative Agreement No. NNA09DA77 A issued by the Office of Space Science).

REFERENCES

- Allamandola, L. J., Sandford, S. A., & Valero, G. J. 1988, *Icarus*, **76**, 225
- Bahr, S., Borodin, A., Höfft, O., Kempter, V., & Allouche, A. 2005, *J. Chem. Phys.*, **122**, 234704
- Bahr, S., Toubin, C., & Kempter, V. 2008, *J. Chem. Phys.*, **128**, 134712
- Bakker, B. L. G., & Parker, D. H. 2000, *Chem. Phys. Lett.*, **330**, 293
- Bennett, C. J., Chen, S.-H., Sun, B.-J., Chang, A. H. H., & Kaiser, R. I. 2007, *ApJ*, **660**, 1588
- Bennett, C. J., Jamieson, C. S., & Kaiser, R. I. 2009a, *ApJS*, **182**, 1
- Bennett, C. J., Jamieson, C. S., & Kaiser, R. I. 2009b, *Phys. Chem. Chem. Phys.*, **11**, 4210
- Bennett, C. J., Jamieson, C. S., Mebel, A. M., & Kaiser, R. I. 2004, *Phys. Chem. Chem. Phys.*, **6**, 735
- Bennett, C. J., Jamieson, C. S., Osamura, Y., & Kaiser, R. I. 2005, *ApJ*, **624**, 1097
- Bennett, C. J., & Kaiser, R. I. 2007, *ApJ*, **660**, 1289
- Bergren, M. S., Schuh, D., Sceats, M. G., & Rice, S. A. 1978, *J. Chem. Phys.*, **69**, 3477
- Bisschop, S. E., Fuchs, G. W., Boogert, A. C. A., van Dishoeck, E. F., & Linnartz, H. 2007a, *A&A*, **470**, 749
- Bisschop, S. E., Fuchs, G. W., van Dishoeck, E. F., & Linnartz, H. 2007b, *A&A*, **474**, 1061
- Bisschop, S. E., Jørgensen, J. K., van Dishoeck, E. F., & de Wachter, E. B. M. 2007c, *A&A*, **465**, 913
- Bockelée-Morvan, D., et al. 2000, *A&A*, **353**, 1101
- Boogert, A. C. A., et al. 2008, *ApJ*, **678**, 985
- Bottinelli, S., Ceccarelli, C., Williams, J. P., & Lefloch, B. 2007, *A&A*, **463**, 601
- Bouwman, J., Ludwig, W., Awad, Z., Öberg, K. I., Fuchs, G. W., van Dishoeck, E. F., & Linnartz, H. 2007, *A&A*, **476**, 995
- Chiar, J. E., Adamson, A. J., Kerr, T. H., & Whittet, D. C. B. 1994, *ApJ*, **426**, 240
- Chiar, J. E., Adamson, A. J., Kerr, T. H., & Whittet, D. C. B. 1995, *ApJ*, **455**, 234
- Chiar, J. E., Gerakines, P. A., Whittet, D. C. B., Pendleton, Y. J., Tielens, A. G. G. M., Adamson, A. J., & Boogert, A. C. A. 1998, *ApJ*, **498**, 716
- Collings, M. P., Dever, J. W., Fraser, H. J., & McCoustra, M. R. S. 2003a, *Astrophys. Space Sci.*, **285**, 633
- Collings, M. P., Dever, J. W., Fraser, H. J., McCoustra, M. R. S., & Williams, D. A. 2003b, *ApJ*, **583**, 1058
- Ehrenfreund, P., Boogert, A. C. A., Gerakines, P. A., Jansen, D. J., Schutte, W. A., Tielens, A. G. G. M., & van Dishoeck, E. F. 1996, *A&A*, **312**, 263
- Falk, M. 1987, *J. Chem. Phys.*, **86**, 560
- Forney, D., Jacox, M. E., & Thompson, W. E. 2003, *J. Chem. Phys.*, **119**, 10814
- Frenklach, M. 1984, *Combust. Flame*, **58**, 69
- Frenklach, M., Packard, A., & Feeley, R. 2007, in *Modeling of Chemical Reactions*, ed. R. W. Carr (Elsevier Series Comprehensive Chemical Kinetics, Vol. 42; Amsterdam: Elsevier), 243
- Frenklach, M., Wang, H., & Rabinowitz, M. J. 1992, *Prog. Energy Combust. Sci.*, **18**, 47
- Froben, F. W., Rabin, I., Ritz, M., & Schulze, W. 1996, *Z. Phys. D*, **38**, 335
- Gale, G. M., Guyot-Sionnest, P., Zheng, W. Q., & Flytzanis, C. 1985, *Phys. Rev. Lett.*, **54**, 823
- Garrod, R. T., & Herbst, E. 2006, *A&A*, **457**, 927
- Gerakines, P. A., & Moore, M. H. 2001, *Icarus*, **154**, 372
- Gerakines, P. A., Schutte, W. A., & Ehrenfreund, P. 1996, *A&A*, **312**, 289
- Gerakines, P. A., Schutte, W. A., Greenberg, J. M., & van Dishoeck, E. F. 1995, *A&A*, **296**, 810
- Gibb, E. L., Whittet, D. C. B., Boogert, A. C. A., & Tielens, A. G. G. M. 2004, *ApJS*, **151**, 35
- Goumans, T. P. M., Uppal, M. A., & Brown, W. A. 2008, *MNRAS*, **384**, 1158
- Harvey, K. B., & Ogilvie, J. F. 1962, *Can. J. Chem.*, **40**, 85
- Hidaka, H., Kouchi, A., & Watanabe, N. 2007, *J. Chem. Phys.*, **126**, 204707
- Hovington, P., Drouin, D., & Gauvin, R. 1997, *Scanning*, **19**, 1

- Hudson, R. L., & Moore, M. H. 1999, *Icarus*, **140**, 451
- Hudson, R. L., & Moore, M. H. 2000, *Icarus*, **145**, 661
- Hudson, R. L., & Moore, M. H. 2001, *J. Geophys. Res.*, **106**, 33275
- Ikeda, M., Ohishi, M., Nummelin, A., Dickens, J. E., Bergman, P., Hjalmarson, Å., & Irvine, W. M. 2001, *ApJ*, **560**, 792
- Irvine, W. M., Friberg, P., Kaifu, N., Mathews, H. E., Minh, Y. C., Ohisi, M., & v Ishikawa, S. 1990, *A&A*, **229**, L9
- Jamieson, C. S., Mebel, A. M., & Kaiser, R. I. 2006, *ApJS*, **163**, 184
- Jenniskens, P., Blake, D. F., & Kouchi, A. 1998, in *Amorphous Water Ice. A Solar System Material*, ASSL Vol. 227: Solar System Ices, ed. B. Schmitt et al. (Dordrecht: Kluwer), 139
- Jiang, G. J., Person, W. B., & Brown, K. G. 1975, *J. Chem. Phys.*, **64**, 1201
- Johnson, R. E. 1990, *Energetic Charged-Particle Interactions with Atmospheres and Surfaces* (Berlin: Springer)
- Kaiser, R. I. 2002, *Chem. Rev.*, **102**, 1309
- Kaiser, R. I., Eich, G., Gabrysch, A., & Roessler, K. 1997, *ApJ*, **484**, 487
- Keane, J. V., Tielens, A. G. G. M., Boogert, A. C. A., Schutte, W. A., & Whittet, D. C. B. 2001, *A&A*, **376**, 254
- Kizhakevariam, N., Villegas, I., & Weaver, M. J. 1995, *J. Phys. Chem.*, **99**, 7677
- Lattanzi, V., Walters, A., Drouin, B. J., & Pearson, J. C. 2008, *ApJS*, **176**, 536
- Liu, S.-Y., Girart, J. M., Remijan, A., & Snyder, L. E. 2002, *ApJ*, **576**, 255
- Liu, S.-Y., Mehringer, D. M., & Snyder, L. E. 2001, *ApJ*, **552**, 654
- Madzunkov, S. M., MacAskill, J. A., Chutjian, A., Ehrenfreund, P., Darrach, M. R., Vidali, G., & Shortt, B. J. 2009, *ApJ*, **697**, 801
- Maeda, S., & Ohno, K. 2008, *Chem. Phys. Lett.*, **460**, 55
- Mastrapa, R. M., Sandford, S. A., Roush, T. L., Cruikshank, D. P., & Dalle Ore, C. M. 2009, *ApJ*, **701**, 1347
- Mathis, J. S., Mezger, P. G., & Panagia, N. 1983, *A&A*, **128**, 212
- Milligan, D. E., & Jacox, M. E. 1971, *J. Chem. Phys.*, **54**, 927
- Millikan, R. C., & Pitzer, K. S. 1958, *J. Am. Chem. Soc.*, **80**, 3515
- Mohammed, H. H. 1990, *J. Chem. Phys.*, **93**, 412
- Oba, Y., Watanabe, N., Kouchi, A., Hama, T., & Pirronello, V. 2010, *ApJ*, **712**, L174
- Ockman, N. 1958, *Adv. Phys.*, **7**, 199
- Okabe, H. 1978, *Photochemistry of Small Molecules* (New York: Wiley)
- Parkinson, C. D., Liang, M.-C., Hartman, H., Hansen, C. J., Tinetti, G., Meadows, V., Kirschvink, J. L., & Yung, Y. L. 2007, *A&A*, **463**, 353
- Prasad, S. S., & Tarafdar, S. P. 1983, *ApJ*, **267**, 603
- Requena-Torres, M. A., Marcelino, N., Jiménez-Serra, I., Martín-Pintado, J., Martín, S., & Mauersberger, R. 2007, *ApJ*, **655**, L37
- Requena-Torres, M. A., Martín-Pintado, J., Rodríguez-Franco, A., Martín, S., Rodríguez-Fernández, N. J., & de Vicente, P. 2006, *A&A*, **455**, 971
- Ritzhaupt, G., Collier, W. B., Thornton, C., & d Devlin, J. P. 1980, *Chem. Phys. Lett.*, **70**, 294
- Schutte, W. A., et al. 1999, *A&A*, **343**, 966
- Slanger, T. G., & Black, G. 1982, *J. Chem. Phys.*, **77**, 2432
- Song, X., Li, J., Hou, H., & Wang, B. 2006, *J. Chem. Phys.*, **125**, 094301
- Spinks, J. W. T., & Woods, R. J. 1990, *Introduction to Radiation Chemistry* (3rd ed.; New York: John Wiley and Sons)
- Stief, L. J., Payne, W. A., & Klemm, R. B. 1975, *J. Chem. Phys.*, **62**, 4000
- Strazzulla, G., & Johnson, R. E. 1991, in *Comets in the Post-Halley Era*, ed. R. Newburn, Jr., M. Neugebauer, & J. Rahe (Dordrecht: Kluwer), 243
- Talbi, D., Chandler, G. S., & Rohl, A. L. 2006, *Chem. Phys.*, **320**, 214
- Tielens, A. G. G. M., Tokunaga, A. T., Geballe, T. R., & Baas, F. 1991, *ApJ*, **381**, 181
- Tso, T. L., & Lee, E. K. C. 1984, *J. Phys. Chem.*, **88**, 5475
- Turner, B. E., Terzieva, R., & Herbst, E. 1999, *ApJ*, **518**, 699
- Vigren, E., et al. 2010, *ApJ*, **709**, 1429
- Watanabe, N., Mouri, O., Nagaoka, A., Chigai, T., Kouchi, A., & Pirronello, V. 2007, *ApJ*, **668**, 1001
- Watanabe, N., Shiraki, T., & Kouchi, A. 2003, *ApJ*, **588**, L121
- Whittet, D. C. B., Bode, M. F., Baines, D. W. T., Longmore, A. J., & Evans, A. 1983, *Nature*, **303**, 218
- Whittet, D. C. B., Longmore, A. J., & McFadzean, A. D. 1985, *MNRAS*, **216**, 45P
- Zelsmann, H. R., Marechal, Y., Chosson, A., & Faure, P. 1975, *J. Mol. Struct.*, **29**, 357
- Zheng, W., Jewitt, D., & Kaiser, R. I. 2006, *ApJ*, **639**, 534
- Zheng, W., Jewitt, D., & Kaiser, R. I. 2007, *Chem. Phys. Lett.*, **435**, 289
- Zheng, W., & Kaiser, R. I. 2007, *Chem. Phys. Lett.*, **450**, 55
- Zuckerman, B., Ball, J. A., & Gottlieb, C. A. 1971, *ApJ*, **163**, L41